Proceedings of Global Power and Propulsion Society
ISSN-Nr: 2504-4400
GPPS Xi'an21
18th – 20th October, 2021
www.gpps.global

GPPS-TC-2021-0195

Prediction of Engine Intake Noise with Discontinuous Least-Square Finite Element Method in Frequency Domain Acoustics

Weidong Shao
1. AECC Commercial Aircraft Engine Co., Ltd.
2. Shanghai Key Laboratory of Aircraft Engine Digital Twin
shilin1225@126.com
Shanghai, China

Bo Huang
1. AECC Commercial Aircraft Engine Co., Ltd.
2. Shanghai Key Laboratory of Aircraft Engine Digital Twin
huangbo_acae@163.com
Shanghai, China

Xinwen Zhang
AECC Commercial Aircraft Engine Co., Ltd.
1455212096@qq.com
Shanghai, China

Changchun Liu
AECC Commercial Aircraft Engine Co., Ltd.
liuchangchun@acae.com.cn
Shanghai, China

Bing Lin
AECC Commercial Aircraft Engine Co., Ltd.
linbing_work@163.com
Shanghai, China

ABSTRACT

In the frame of efficient passive treatment, intake noise prediction needs improving. This paper presents a novel numerical method for predicting acoustic propagation from axisymmetric ducted fans of high bypass ratio turbofan engine. Non-uniform mean flow convection and acoustic liner treatment is included. The linearized Euler equations are solved in the frequency domain. The spatial discretization is conducted with the discontinuous least-square finite element method so that the resulting algebraic equation is Hermitian conjugate symmetric. Moreover, the high-order accuracy and *hp* refinement is obtained while memory shared parallel computing strategy is used for convergence acceleration. Based on the near field acoustics, the porous Ffowcs Williams-Hawkings equation is solved for far field sound pressure level. Benchmark problems including monopole radiation in uniform mean flow and acoustic propagation in sheared mean flow are used to validate the capability. Simulations of the JT15D static test intake noise are performed, where the far field angle of peak sound pressure level, about 60° agrees well with experimental data and numerical data available in the literature.

1. INTRODUCTION

Airplane noise control technology is one of main goals of green aviation, since the airplane noise not only influences the comfort and communication of passengers, but also leads to secondary community noise during take-off and approach(He, 2010). On one hand, the airplane noise level is dominated by the aircraft noise(Peake and Parry, 2012), including the fan noise, compressor noise, core noise and jet noise, etc. They are mostly generated by the unsteady motion of air/gas in the aircraft engine, accompanying the pressure pulsation propagated to the far field through elasticity and inertia.

On the other hand, pollutants emission decrease technology is also one goal of green aviation. It demands overall efficiency improvement of aircraft propulsion system. The high bypass ratio or ultra-high bypass ratio turbofan architecture is promising. However, the nacelle configured with large diameter fan increases the drag, which is detrimental to the overall efficiency. Then, the nacelle has to be shortened, which results in shorter rotor-stator distance, more significant inlet distortions and less passive treatment(Laborderie and Moreau, 2016). In the frame of efficient passive treatment, the present work aims at improving intake noise prediction.

Computational analysis performed in ducted noise propagation and radiation falls into two broad categories: direct time-domain approach and frequency-domain acoustics approach. Time-domain approach solves directly the linearized Euler equation(Li et al., 2004), even the full Euler or Navier-Stokes equations(Ozyoruk and Long, 1996; Stanescu et al.,

1999). It is able to handle multi-frequency sources in one single computation case. The disadvantage of time-domain approach is related to treatment of frequency-dependent liners. Although there were some improvement of time-domain impedance boundary condition, such as z-transform(Ozyoruk et al., 1998), Helmholtz resonator model(Rienstra, 2006), first and second order response systems model(Reymen et al., 2008), the character of liner could be changed or even wrong. Moreover, when the prescribed mean flow contains a strong shear layer, time-domain approach easily forms physical Kelvin-Helmholtz instabilities, which can grow boundlessly, i.e. diverged solution. In order to overcome the numerical instabilities, strategies including gradient term suppression(Zhang et al., 2004), gradient term filtering(Zhang et al., 2014), acoustic perturbation equations(Bui et al., 2009; Ewert et al., 2011), linearized Navier-Stokes equations(Gikadi et al., 2014; Sun et al., 2018), has been adopted. However, the accuracy and increased computational cost still needs balancing.

Frequency-domain acoustics approach solves the controlling equation with the Fourier transform. The obvious advantage is easy incorporation of solving strategy and impedance boundary condition. Moreover, the absolute stability of frequency-domain acoustics approach has been demonstrated(Agarwal et al., 2004). Based on the Galerkin method, solving the velocity potential equation in the frequency domain has wide application(Nallasamy et al., 2000; Roy and Eversman, 2001). With fourth-order finite difference spatial discretization and pseudo time marching, axisymmetric linearized Euler equation and Myers soft boundary condition(Myers, 1980) was solved(Ozyoruk et al., 2004). By solving the two-dimensional linearized Euler equation, streamline upwind Galerkin method and discontinuous Galerkin method were compared(Rao and Morris, 2006). When triangular meshes and nodal interpolation are used, the former is superior to the latter. With irrotational and homentropic mean flow, the linearized mass flow equation was solved with hybrid finite element method(Duta et al., 2005; Duta and Giles, 2006). Through streamline upwind Galerkin method and automatic code differentiation, the linearized Navier-Stokes equation was solved with a homogeneous Dirichlet boundary condition(Bissuel et al., 2018). Although non-uniform mean flow and liner impedance character were considered, the spatial discretization order is low, leading to more degrees of freedom per wavelength. In addition, the adaptive refinement is limited.

The goal of this paper is to describe a recently developed, parallel, frequency-domain acoustics code, including background flow refraction effects and passive treatment effects. The discontinuous least-square method is used to guarantee the Hermitian conjugate symmetric of resulting linear algebraic equation. Though the code is suitable for both fore and aft radiation, the present approach has been applied only to fore-propagation problems in this paper.

The remainder of this paper is organized as follows. In Section 2, the linearized Euler equation in axisymmetric flow and boundary conditions are described. The discontinuous least-square method is applied to the controlling equation and the far field solution strategy is presented in Section 3. Then, the benchmark problems and JT15D static test intake noise simulation are used to verify the code in Section 4. Finally, the conclusions are drawn in Section 5.

2. MATHEMATICAL MODEL

2.1 Controlling Equation

Consider the axisymmetric, time-dependent, linearized Euler equations, written in non-dimensional, non-conservative, in cylindrical coordinates

$$\left[\frac{\partial}{\partial t}+\mathbf{B}_x\frac{\partial}{\partial x}+\mathbf{B}_R\frac{\partial}{\partial R}+\mathbf{B}_\theta\frac{\partial}{\partial \theta}+\mathbf{B}\right]\tilde{\boldsymbol{Q}}=\boldsymbol{S}\,, \tag{1}$$

$$\tilde{\boldsymbol{Q}}=[\tilde{\rho}\quad \tilde{u}_x\quad \tilde{u}_R\quad \tilde{u}_\theta\quad \tilde{p}]^T\,. \tag{2}$$

where t is time, x, R, θ are coordinate directions, respectively; ρ, p are density and pressure, which are connected by the equation of state; u_x, u_R, u_θ are velocity in coordinate directions; $\mathbf{B}_x$, $\mathbf{B}_R$, $\mathbf{B}_\theta$ are coefficient matrix, presented in Appendix A; $\boldsymbol{S}$ is the source term. The tilde on a variable indicates the perturbation while the bar on a variable indicates the mean.

Eq. (1) is transformed into the frequency-domain by assuming perturbations of the primitive-dependent variables are of the form

$$\tilde{\boldsymbol{Q}}=\int\sum_{m=-\infty}^{\infty}\hat{\boldsymbol{Q}}\exp\left[i\left(m\theta+\omega t\right)\right]d\omega\,, \tag{3}$$

$$\hat{\boldsymbol{Q}}=[\hat{\rho}\quad \hat{u}_x\quad \hat{u}_R\quad \hat{u}_\theta\quad \hat{p}]^T\,. \tag{4}$$

where m, ω are the azimuthal mode number and circular frequency, respectively; $i^2+1=0$. The hat on a variable indicates a complex quantity.

The resulting frequency-domain equation is written

$$\left[\mathbf{B}_x\frac{\partial}{\partial x}+\mathbf{B}_R\frac{\partial}{\partial R}+im\mathbf{B}_\theta+\mathbf{B}+i\omega\mathbf{I}\right]\hat{\boldsymbol{Q}}=\hat{\boldsymbol{S}}\,. \tag{5}$$

Hence, the three-dimensional acoustic field of single spinning mode needs solving only in projected two-dimensional space instead, reducing significantly the computational cost of full three-dimensional simulation. In some literature(Duta et al., 2005; Duta and Giles, 2006), a standard finite element discretisation of the acoustic field is combined with a Fourier spectral representation in the circumferential direction. The difference is that they solved only the mass conservation equation.

2.2 Boundary Conditions

2.2.1 Far field conditions

The non-reflecting far field boundary should transport smoothly the entropy, vorticity and acoustic waves through the boundary without artificial reflection. The radiation operator(Tam and Webb, 1993) is used for pressure perturbation only when the advection velocity component projected on the outward normal remains positive. The far field boundary condition is written in frequency-domain and cylindrical coordinates

$$\left[V\frac{x-x_s}{|\boldsymbol{r}|}\mathbf{I}\frac{\partial}{\partial x}+V\frac{R-R_s}{|\boldsymbol{r}|}\mathbf{I}\frac{\partial}{\partial R}+\left(\frac{V}{|\boldsymbol{r}|}+i\omega\right)\mathbf{I}\right]\hat{\boldsymbol{Q}}=\mathbf{0}, \tag{6}$$

$$V=\bar{\boldsymbol{u}}\cdot\frac{\boldsymbol{r}}{|\boldsymbol{r}|}+\sqrt{\frac{\gamma\bar{p}}{\bar{\rho}}-\left[\bar{\boldsymbol{u}}-\left(\bar{\boldsymbol{u}}\cdot\frac{\boldsymbol{r}}{|\boldsymbol{r}|}\right)\frac{\boldsymbol{r}}{|\boldsymbol{r}|}\right]^2}\,. \tag{7}$$

where x_s, R_s are the presupposed acoustic source coordinates, respectively; $\boldsymbol{r}$=(x-x_s, R-R_s, 0).

2.2.2 Axis Conditions

Due to R=0 on the axis, the singularity can be overcome through asymptotic analysis. The asymptotic solution close to the axis is

$$\begin{cases}\hat{u}_R=\hat{u}_\theta\approx 0 & m=0\\ \hat{\rho}=\hat{u}_x=i\hat{u}_\theta+\mathrm{sgn}(m)\hat{u}_R=\hat{p}\approx 0 & |m|=1\\ \hat{\boldsymbol{Q}}\approx\mathbf{0} & |m|\geq 2\end{cases}. \tag{8}$$

Thus, close to the axis any term in Eq.(5) with R on the denominator should be replaced by its derivative.

According to the spinning mode, the boundary condition on the axis is

$$\left[\mathbf{A}_R\frac{\partial}{\partial R}+\mathbf{I}-\mathbf{A}_R\right]\hat{\boldsymbol{Q}}=\mathbf{0}, \tag{9}$$

$$\mathbf{A}_R=diag\left[\frac{1+(-1)^m}{2}\quad\frac{1-(-1)^m}{2}\quad\frac{1-(-1)^m}{2}\quad\frac{1-(-1)^m}{2}\quad\frac{1+(-1)^m}{2}\right]. \tag{10}$$

where *diag* indicates the diagonal matrix.

2.2.3 Impedance Conditions

With passive treatment of nacelle intake, the liner is described with impedance condition(Myers, 1980). The matrix form of boundary condition in frequency-domain can be written as follows

$$\left[\mathbf{L}_x\frac{\partial}{\partial x}+\mathbf{L}_R\frac{\partial}{\partial R}+\mathbf{L}\right]\hat{\boldsymbol{Q}}=\mathbf{0}\,. \tag{11}$$

where the coefficient matrix $\mathbf{L}_x$, $\mathbf{L}_R$, $\mathbf{L}$ is presented in Appendix A. Note, when the impedance is set to infinity, the impedance condition is turned to hard wall conditions.

2.2.4 Fan Face Conditions

In industrial simulations, the acoustic source information at the fan face is given by exact cylindrical duct eigensolutions. It is assumed that the mean flow at the fan face is uniform and the shroud and the hub are hard wall. Then, the acoustic pressure of a circular annular duct is analytical, i.e.

$$\hat{p}=\begin{cases}a & k_{mn}=0, m=0\\ a_{mn}\left[J_m(k_{mn}R)-\dfrac{J'_m(k_{mn}R_o)}{Y'_m(k_{mn}R_o)}Y_m(k_{mn}R)\right] & k_{mn}\neq 0\end{cases}, \tag{12}$$

$$J'_m(k_{mn}R_i)Y'_m(k_{mn}R_o)-J'_m(k_{mn}R_o)Y'_m(k_{mn}R_i)=0\,. \tag{13}$$

where m, n are the azimuthal and radial mode orders, respectively; k_{mn} are the eigenvalues; a and a_{mn} are the amplitude; R_i, R_o are the inner and outer radius of annular duct, respectively; J_m, Y_m mean the m-th order Bessel functions of the first and second kinds, respectively. The prime indicate the derivative.

The mode decomposition is made using the rotor-stator interaction theory(Tyler and Sofrin, 1962). The propagation direction of modes is determined by the group velocity. Thus, the inflow modes are set to the given eigensolutions while the outflow modes pass smoothly through the boundary. The resulting matrix form of fan face condition is

$$\left[\mathbf{F}_R \frac{\partial}{\partial R} + \mathbf{F}\right]\hat{\boldsymbol{Q}} = \boldsymbol{q}_s \cdot \tag{14}$$

where the coefficient matrix $\mathbf{F}_R$, $\mathbf{F}$ and source term $\boldsymbol{q}_s$ are presented in Appendix A.

Although the fan face condition is theoretically non-reflecting, numerical experiments have shown that it does not eliminate completely the reflecting wave modes. Specifying the given mode distribution at the fan face for some cases performs better.

3. NUMERICAL METHOD

3.1 Unified Form

In order to discretize the controlling equation in a simple and concise style, the mathematical problem is written in a unified form

$$\begin{bmatrix}\mathbf{U}^I \\ \mathbf{U}^B\end{bmatrix}\hat{\boldsymbol{Q}} = \begin{bmatrix}\boldsymbol{S}^I \\ \boldsymbol{S}^B\end{bmatrix}, \tag{15}$$

$$\begin{bmatrix}\mathbf{U}^I \\ \mathbf{U}^B\end{bmatrix} = \begin{bmatrix}\mathbf{U}_x^I \\ \mathbf{U}_x^B\end{bmatrix}\frac{\partial}{\partial x} + \begin{bmatrix}\mathbf{U}_R^I \\ \mathbf{U}_R^B\end{bmatrix}\frac{\partial}{\partial R} + \begin{bmatrix}\mathbf{U}_C^I \\ \mathbf{U}_C^B\end{bmatrix}. \tag{16}$$

where $\mathbf{U}$ means the linear operator and $\boldsymbol{S}$ means the source terms. The superscript I indicates the interior domain while the superscript B indicates the boundary. The detailed forms of operators in Eq.(16) are presented in Section 2.

3.2 Discretization Schemes

For problem Eq.(15), the discontinuous least-square method is to find the approximate solution in the square-integral space with the following equivalent optimization problem

$$\min Er\left(\hat{\boldsymbol{Q}}\right) = \int_\Omega w_I \left|\mathbf{U}^I\hat{\boldsymbol{Q}} - \boldsymbol{S}^I\right|^2 d\Omega + \int_{\partial\Omega} w_B \left|\mathbf{U}^B\hat{\boldsymbol{Q}} - \boldsymbol{S}^B\right|^2 d\partial\Omega + \int_\Gamma w_N \left|\left\langle\hat{\boldsymbol{Q}}\right\rangle\right|^2 d\Gamma \cdot \tag{17}$$

where w_I, w_B, w_N mean the interior domain integral weight, the boundary integral weight, and the discontinuous contact integral weight, respectively. The symbol < > indicates the difference between values on the discontinuous contact interface.

The computational domain is partitioned into non-overlapping regions. According to the variational principle, Eq.(17) is transformed to

$$\begin{aligned}&\int_\Omega w_I\left[\mathbf{U}^I\delta\hat{\boldsymbol{Q}}\right]^{T^*}\mathbf{U}^I\hat{\boldsymbol{Q}}d\Omega + \int_{\partial\Omega} w_B\left[\mathbf{U}^B\delta\hat{\boldsymbol{Q}}\right]^{T^*}\mathbf{U}^B\hat{\boldsymbol{Q}}d\partial\Omega + \int_\Gamma w_N\left\langle\delta\hat{\boldsymbol{Q}}\right\rangle^{T^*}\left\langle\hat{\boldsymbol{Q}}\right\rangle d\Gamma = \\ &\int_\Omega w_I\left[\left(\boldsymbol{S}^I\right)^{T^*}\mathbf{U}^I\delta\hat{\boldsymbol{Q}}\right]^{T^*}d\Omega + \int_{\partial\Omega} w_B\left[\left(\boldsymbol{S}^B\right)^{T^*}\mathbf{U}^B\delta\hat{\boldsymbol{Q}}\right]^{T^*}d\partial\Omega\end{aligned} \tag{18}$$

where $\delta\hat{\boldsymbol{Q}}$ represents the variational space. The resulting system is Hermitian conjugate symmetric.

3.3 Finite Element Space

The solution vector is approximated by

$$\hat{\boldsymbol{Q}} = \sum_{h=1}^{NE}\hat{\boldsymbol{Q}}^h, \quad \hat{\boldsymbol{Q}}^h \approx \sum_{k=1}^{NB}\psi_k^h\hat{\boldsymbol{Q}}_k^h \cdot \tag{19}$$

where NE means the number of elements; NB means the number of basis function within each element. In this paper, the basis function is chosen by analogy with the Taylor series

$$\psi_k^h = \begin{cases}1 & k=1 \\ \phi_k^h - \frac{1}{A^h}\int_{\Omega^h}\phi_k^h d\Omega & k\geq 2\end{cases}, \quad \phi_k^h(x,R) = \frac{1}{i!}\frac{1}{j!}\left(\frac{x-x_c}{\Delta x}\right)^i\left(\frac{R-R_c}{\Delta R}\right)^j \cdot \tag{20}$$

where A^h is the element area; x_c, R_c are the barycentric coordinates, respectively; Δx, ΔR are the half span of element in two directions, respectively. The index k is obtained by counting the number of pairs with the limit: i+j≤NO. NO is the element discretization order.

3.4 Algebraic Equation

Inserting Eq.(19) into Eq.(18) results in the linear algebraic equation

$$\mathbf{A}\boldsymbol{x} = \boldsymbol{b}. \tag{21}$$

where **A** is a Hermitian positive definite complex matrix, $\boldsymbol{x}$ is the solution vector. The complex conjugate gradient method is used to Eq.(21). Moreover, the block Jacobi preconditioner is used. When the underlying physics is relatively simple, the standard Jacobi preconditioner is recommended because this preconditioner is easy to obtain.

3.5 Parallel Computing

The shared memory approach is used with the OpenMP standard. The parallel domain is exerted on the most outer loops. The numerical experiment shows that the efficiency of parallel computing reaches more than 88% with the computing cores not larger than 64.

3.5 Porous FW-H analogy

The far field is solved with the Ffowcs Williams-Hawkings analogy(Ffowcs Williams and Hawkings, 1969) with its time-domain porous form

$$\left\{\frac{D^2}{Dt^2}-c_\infty^2\nabla^2\right\}\left[(\rho-\rho_\infty)H(f)\right]=\frac{D}{Dt}\left[Q\delta(f)\right]-\frac{\partial}{\partial x_i}\left[L_i\delta(f)\right]+\frac{\partial^2}{\partial x_i\partial x_j}\left[T_{ij}H(f)\right], \tag{22}$$

$$\frac{D}{Dt}=\frac{\partial}{\partial t}+U_{\infty,i}\frac{\partial}{\partial x_i}\cdot \tag{23}$$

where H is the Heaviside function; δ is the Dirac function; U and c are the flow velocity and sonic velocity, respectively; Q, L_i, T_{ij} mean the monopole source, dipole source and quadrupole source, respectively. The subscript ∞ indicates the infinity.

The far field pressure in the frequency-domain can be obtained

$$\hat{p}=2\pi c_\infty^2\int_{f=0}i\omega\hat{Q}G+\left(U_{\infty,i}\hat{Q}-\hat{L}_i\right)\frac{\partial G}{\partial x_i}dS\cdot \tag{24}$$

where f=0 indicates the porous surface. G is frequency-domain Green function. In Eq.(24), the three-dimensional acoustic field is recovered from the axisymmetric solution with the mode transform.

4. RESULTS AND DISCUSSION

4.1 Monopole Radiation in Uniform Mean Flow

This benchmark problem describes a monopole source in static mean flow, which has an analytical solution. It is used to verify the *hp*-refinement of the presented method. Figure 1 shows the mesh where the blue half circle indicates the porous integral face. The acoustic pressure in the near field is also illustrated, where the wave can pass smoothly the boundary. The non-reflecting boundary is effective.

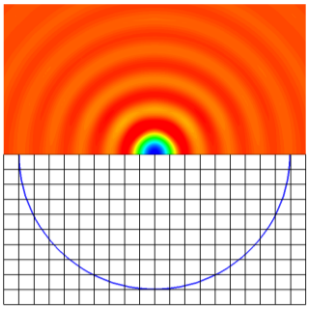

Figure 1 Mesh and Acoustic Pressure of Monopole Radiation in Uniform Mean Flow

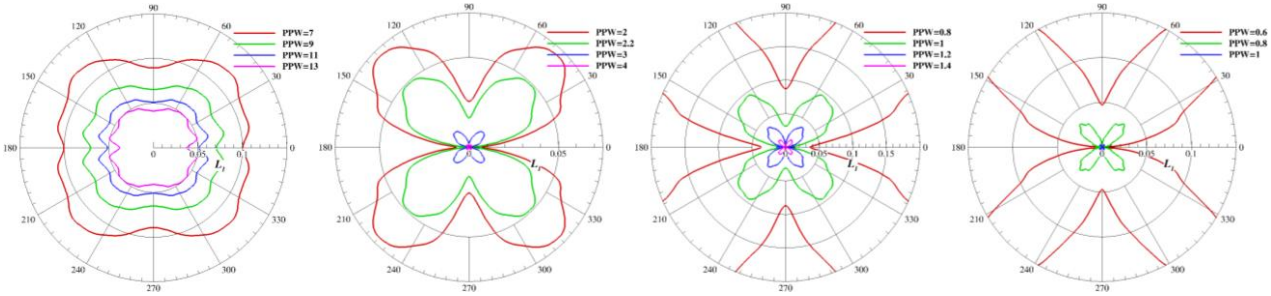

(a) N=2 (b) N=4 (c) N=6 (d) N=8

Figure 2 Relative Error of Far Field Directivity Computed with Different Discretization Order

The far field directivity of monopole radiation with different discretization order is illustrated in Figure 2. For each order, cases with different points per wavelength (PPW) are compared. The sound pressure level(SPL) error relative to analytical SPL decreases as PPW increases. Moreover, high order discretization needs less PPW than low order discretization. For the 5% relative error, the PPW is 1 when the discretization order reaches 6.

4.2 Acoustic Propagation in Sheared Mean Flow

This benchmark problem describes acoustic propagation from monopole source in sheared mean flow. The detail is given in the literature(Agarwal et al., 2004) and m=0 is chosen here. Using its analytical solution, the numerical stability of the presented method can be verified. Figure 3 shows the case mesh and acoustic pressure distribution. In addition, the comparison between numerical solution and analytical are compared. Since the sheared mean flow is at the far outflow boundary, the reflecting artificial wave pattern is observed, which can be overcome using larger computational domain. Moreover, the instability wave along the symmetry plane is removed.

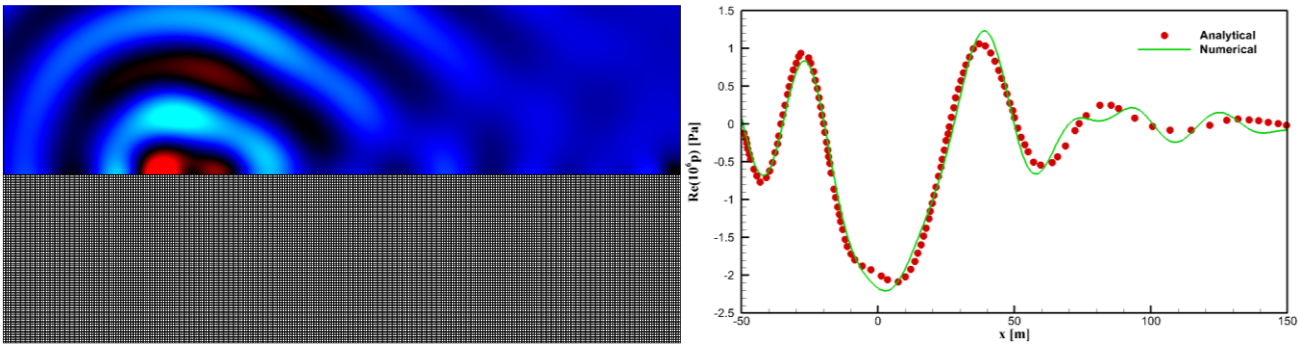

(a) Mesh and Acoustic Pressure Contour (b) Comparison between Numerical and Analytical

Figure 3 Mesh and Acoustic Pressure Contour of Acoustic Propagation in Sheared Mean Flow

4.3 JT15D intake noise

JT15D intake noise at static test facility is widely used to validate the accuracy of numerical method(Lan et al., 2004). This problem has experiment data and other simulation results. Figure 4 shows the propagation of forward noise from rotor-stator interaction with mode(-13,1) and blade passing frequency 3150Hz. The refraction effect near the tip is clearly seen. Figure 5 illustrates the comparison of far field directivity between different studies. Obviously, the present method can accurately capture the directivity. However, the discrepancy of SPL under the condition of passive treatment may be the uncertainty in liner impedance characteristics.

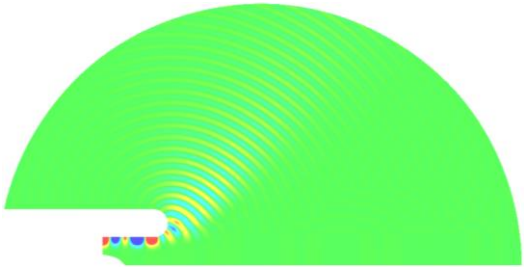

Figure 4 Acoustic Pressure Contour of JT15D Intake Noise with Hard Wall

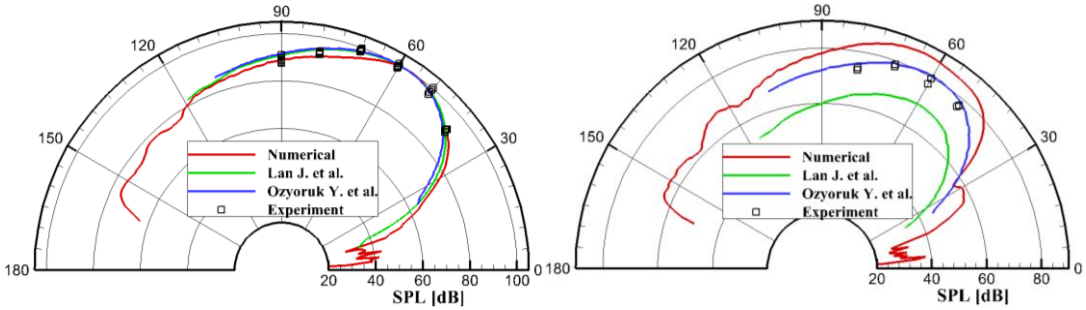

(a) Far Field Directivity with Hard Wall (b) Far Field Directivity with Liner

Figure 5 Comparison of Far Field Directivity with Different Wall Conditions

5. CONCLUSIONS

A discontinuous least-square method in the frequency-domain has been developed for predicting ducted acoustic propagation. The linearized Euler equation about an axisymmetric non-uniform mean flow is solved with the presented method. Hermitian conjugate systems are obtained while the resulting algebraic linear equations are positive definite. Shared memory parallel computing is implemented for efficient solution of equations as well as outer loops. Numerical experiments were carried out for monopole radiation in uniform flow and acoustic propagation in sheared mean flow as well as JT15D intake noise. The *hp* refinement of the method is demonstrated. Higher order needs lower points per wavelength with the same accuracy. The absolute stability is also verified. Both the hard wall and attenuation effect of liners are well modelled. The extension to full three-dimensional linearized Navier-Stokes equation is under way.

ACKNOWLEDGMENTS

This study is sponsored by Shanghai Sailing Program(Project No. 20YF1454200) and Natural Science Foundation of Shanghai(Project No. 21ZR1469600).

REFERENCES

[1] Agarwal, A., Morris, P. and Mani, R. (2004). Calculation of Sound Propagation in Nonuniform Flows: Suppression of Instability Waves. *AIAA Journal*, 42(1), pp. 80-88.

[2] Bissuel, A., Allaire, G., Daumas, L., et al. (2018). Linearized Navier-Stokes Equations for Aeroacoustics Using Stabilized Finite Elements: Boundary Conditions and Industrial Application to Aft-Fan Noise Propagation. *Computers and Fluids*, 166(30), pp. 32-45.

[3] Bui, T., Ihme, M., Schroder, W. and Pitsch, H. (2009). Analysis of Different Sound Source Formulations to Simulate Combustion Generated Noise Using a Hybrid Les/Ape-rf Method. *International Journal of Aeroacoustics*, 8(1), pp. 95-123.

[4] Duta, M., Giles, M. (2006). A Three-Dimensional Hybrid Finite Element/Spectral Analysis of Noise Radiation from Turbofan Inlets. *Journal of Sound and Vibration*, 296(6), pp. 623-642.

[5] Duta, M., Laird, A., Giles, M. (2005). Aeroacoustic Analysis Using a Hybrid Finite Element Method. *Proceedings of the Institution of Mechanical Engineers, Part A: Journal of Power and Energy*, 219(6), pp. 413-420.

[6] Ewert, R., Dierke, J., Siebert, J., Neifeld, A., et al. (2011). CAA Broadband Noise Prediction for Aeroacoustic Design. *Journal of Sound and Vibration*, 330(17), pp. 4139-4160.

[7] Ffowes Williams, J. and Hawings, D. (1969). Sound Generation by Turbulence and Surfaces in Arbitrary Motion. *Philosophical Transactions of the Royal Society of London A: Mathematical and Physical Sciences*, 264(1151), pp. 321-342.

[8] Gikadi, J., Foller, S. and Sattelmayer, T. (2014). Impact of Turbulence on the Prediction of Linear Aeroacoustic Interactions: Acoustic Response of a Turbulent Shear Layer. *Journal of Sound and Vibration*, 333(24), pp. 6548-6559.

[9] He, Q. (2010). *Development of an Income-Based Hedonic Monetization Model for the Assessment of Aviation-Related Noise Impacts*. Ph.D. Massachusetts Institute of Technology.

[10] Lan, J., Guo, Y. and Breard, C. (2004). Validation of Acoustic Propagation Code with JT15D Static and Flight Test Data. *The Proceedings of 10th AIAA/CEAS Aeroacoustic Conference*, Manchester, American Institute of Aeronautics and Astronautics, 2986.

[11] Laborderie, J., and Moreau, S. (2016). Prediction of Tonal Ducted Fan Noise. *Journal of Sound and Vibration*, 372(23), pp. 105-132.

[12] Li, X., Schemel, C., Michel, U. and Thiele, F. (2004). Azimuthal Sound Mode Propagation in Axisymmetric Flow Ducts. *AIAA Journal*, 42(10), pp. 2019-2027.

[13] Myers, M. (1980). On the Acoustic Boundary Condition in the Presence of Flow. *Journal of Sound and Vibration*, 71(3), pp. 429-434.

[14] Nallasamy, M., Sutliff, D. and Heidelberg, L. (2000). Propagation of Spinning Acoustic Modes in Turbofan Exhaust Ducts. *Journal of Propulsion and Power*, 16(5), pp. 736-743.

[15] Ozyoruk, Y., Alpman, E., Ahuja, V. and Long, L. (1996). Frequency-Domain Prediction of Turbofan Noise Radiation. *Journal of Sound and Vibration*, 270(4-5), pp. 933-950.

[16] Ozyoruk, Y., and Long, L. (1996). Computation of Sound Radiating from Engine Inlets. *AIAA Journal*, 34(5), pp. 894-901.

[17] Ozyoruk, Y., Long, L. and Jones, M. (1998). Time-Domain Numerical Simulation of a Flow-Impedance Tube. *Journal of Computational Physics*, 146(1), pp. 29-57.

[18] Rao, P. and Morris, P. (2006). Use of Finite Element Methods in Frequency Domain Aeroacoustics. *AIAA Journal*, 44(7), pp. 1643-1652.

[19] Reymen, Y., Baelmans, M. and Desmet, W. (2008). Efficient Implementation of Tam and Auriault's Time-Domain Impedance Boundary Condition. *AIAA Journal*, 46(9), pp. 2368-2376.

[20] Rienstra, S. (2006). Impedance Models in Time Domain, Including the Extended Helmholtz Resonator Model. *The Proceedings of 12th AIAA/CEAS Aeroacoustic Conference*, Boston, American Institute of Aeronautics and Astronautics, 2686.
[21] Roy, I. and Eversman, W. (2001). Far-Field Calculations for Turbofan Noise. *AIAA Journal*, 39(12), pp. 2255-2261.
Peake, N. and Parry, A. (2012). Modern Challenges Facing Turbomachinery Aeroacoustics. *Annual Review of Fluid Mechanics*, 44(1), pp. 227-248.
[22] Stanescu, D., Ait-Ali-Yahia D., Habashi, W. and Robichaud, M. (1999). Multidomain Spectral Computations of Sound Radiation from Ducted Fans. *AIAA Journal*, 37(3), pp. 296-302.
[23] Sun, Y., Fattah, R., Zhong, S. and Zhang, X. (2018). Stable Time-Domain CAA Simulations with Linearized Governing Equations. *Computers and Fluids*, 167(15), pp. 187-195.
[24] Tam, C. and Webb, J. (1993). Dispersion-Relation-Preserving Finite Difference Schemes for Computational Acoustics. *Journal of Computational Physics*, 107(2), pp. 262-281.
[25] Tyler, J. and Sofrin, T. (1962). Axial Flow Compressor Noise Studies. *Transactions of the society of Automotive Engineers*, 70(1), pp. 309-332.
[26] Zhang, X., Chen X., Gill J. and Huang, X. (2014). Gradient Term Filtering for Stable Sound Propagation with Linerized Euler Equations. *The Proceedings of 20th AIAA/CEAS Aeroacoustic Conference*, Boston, American Institute of Aeronautics and Astronautics, 3306.
[27] Zhang, X., Chen X., Morfey C. and Nelson, P. (2004). Computation of Spinning Modal Radiation from an Unflanged Duct. *AIAA Journal*, 42(9), pp. 1795-1801.

APPENDIX A – Coefficient Matrix

The coefficient matrix in the controlling equation are listed as follows

$$\mathbf{B}_x=\begin{bmatrix}\bar{u}_x & \bar{\rho} & 0 & 0 & 0\\ 0 & \bar{u}_x & 0 & 0 & \frac{1}{\bar{\rho}}\\ 0 & 0 & \bar{u}_x & 0 & 0\\ 0 & 0 & 0 & \bar{u}_x & 0\\ 0 & \gamma\bar{p} & 0 & 0 & \bar{u}_x\end{bmatrix},\quad \mathbf{B}_R=\begin{bmatrix}\bar{u}_R & 0 & \bar{\rho} & 0 & 0\\ 0 & \bar{u}_R & 0 & 0 & 0\\ 0 & 0 & \bar{u}_R & 0 & \frac{1}{\bar{\rho}}\\ 0 & 0 & 0 & \bar{u}_R & 0\\ 0 & 0 & \gamma\bar{p} & 0 & \bar{u}_R\end{bmatrix},\quad \mathbf{B}_\theta=\frac{1}{R}\begin{bmatrix}\bar{u}_\theta & 0 & 0 & \bar{\rho} & 0\\ 0 & \bar{u}_\theta & 0 & 0 & 0\\ 0 & 0 & \bar{u}_\theta & 0 & 0\\ 0 & 0 & 0 & \bar{u}_\theta & \frac{1}{\bar{\rho}}\\ 0 & 0 & 0 & \gamma\bar{p} & \bar{u}_\theta\end{bmatrix}, \tag{A1}$$

$$\mathbf{B}=\begin{bmatrix}\frac{\partial\bar{u}_x}{\partial x}+\frac{\partial\bar{u}_R}{\partial R}+\frac{\bar{u}_R}{R} & \frac{\partial\bar{\rho}}{\partial x} & \frac{\partial\bar{\rho}}{\partial R}+\frac{\bar{\rho}}{R} & 0 & 0\\ -\frac{1}{\bar{\rho}^2}\frac{\partial\bar{p}}{\partial x} & \frac{\partial\bar{u}_x}{\partial x} & \frac{\partial\bar{u}_x}{\partial R} & 0 & 0\\ -\frac{1}{\bar{\rho}^2}\frac{\partial\bar{p}}{\partial R} & \frac{\partial\bar{u}_R}{\partial x} & \frac{\partial\bar{u}_R}{\partial R} & -2\frac{\bar{u}_\theta}{R} & 0\\ 0 & \frac{\partial\bar{u}_\theta}{\partial x} & \frac{\partial\bar{u}_\theta}{\partial R}+\frac{\bar{u}_\theta}{R} & \frac{\bar{u}_R}{R} & 0\\ 0 & \frac{\partial\bar{p}}{\partial x} & \frac{\gamma\bar{p}}{R}+\frac{\partial\bar{p}}{\partial R} & 0 & \gamma\left(\frac{\partial\bar{u}_x}{\partial x}+\frac{\partial\bar{u}_R}{\partial R}+\frac{\bar{u}_R}{R}\right)\end{bmatrix}. \tag{A2}$$

where γ is the specific heat ratio.

The coefficient matrix in the impedance condition are listed as follows

$$\mathbf{L}_x=\begin{bmatrix}0&0&0&0&0\\0&0&0&0&0\\0&0&0&0&0\\0&0&0&0&0\\0&0&0&0&A\bar{u}_x\end{bmatrix},\quad \mathbf{L}_R=\begin{bmatrix}0&0&0&0&0\\0&0&0&0&0\\0&0&0&0&0\\0&0&0&0&0\\0&0&0&0&A\bar{u}_R\end{bmatrix},\quad \mathbf{L}=\begin{bmatrix}0&0&0&0&0\\0&0&0&0&0\\0&0&0&0&0\\0&0&0&0&0\\0&-i\omega n_x&-i\omega n_R&0&(\mathbf{L})_{55}\end{bmatrix}, \tag{A3}$$

$$(\mathbf{L})_{55}=i\omega A+\bar{u}_x\frac{\partial A}{\partial x}+\bar{u}_R\frac{\partial A}{\partial R}+\frac{\bar{u}_\theta}{R}\frac{\partial A}{\partial\theta}-A\left[n_x^2\frac{\partial\bar{u}_x}{\partial x}+n_xn_R\left(\frac{\partial\bar{u}_x}{\partial R}+\frac{\partial\bar{u}_R}{\partial x}\right)+n_R^2\frac{\partial\bar{u}_R}{\partial R}-\frac{im\bar{u}_\theta}{R}\right]. \tag{A4}$$

where A is the admittance; n_x, n_R are the outward normal coordinates, respectively.

The coefficient matrix in the fan face condition are listed as follows

$$[\mathbf{F}_B]_{n'n}=i\left(k_{x,mn'}-k_{x,mn}\right)\hat{\boldsymbol{Q}}^L_{mn'}\mathbf{B}_R^{-1}\mathbf{B}_x\hat{\boldsymbol{Q}}^R_{mn}\exp\left[ik_{x,mn}x\right], \tag{A5}$$

$$(\mathbf{F}_R)_j=\left(\mathbf{F}_B^{-1}\begin{bmatrix}\hat{\boldsymbol{Q}}^L_{m1} & \hat{\boldsymbol{Q}}^L_{m2} & \cdots & \hat{\boldsymbol{Q}}^L_{mN}\end{bmatrix}^T\right)_{row(j)}, \tag{A6}$$

$$(\mathbf{F})_j=\left(\mathbf{F}_B^{-1}\left\{-\frac{\partial}{\partial R}\begin{bmatrix}\hat{\boldsymbol{Q}}^L_{m1} & \hat{\boldsymbol{Q}}^L_{m2} & \cdots & \hat{\boldsymbol{Q}}^L_{mN}\end{bmatrix}^T\right\}\right)_{row(j)}, \tag{A7}$$

$$(\boldsymbol{f}_{BG})_{n'} = \left[\hat{\boldsymbol{Q}}^{L}_{mn'} \frac{\partial}{\partial R} - \frac{\partial \hat{\boldsymbol{Q}}^{L}_{mn'}}{\partial R} \right] \boldsymbol{Q}_{BG}, \tag{A8}$$

$$\boldsymbol{q}_{BG} = \mathbf{F}_B^{-1} \boldsymbol{f}_{BG}, \quad (\boldsymbol{q}_s)_j = (\boldsymbol{q}_{BG})_{row(j)}, \; j = 1, 2, \ldots, N_R . \tag{A9}$$

where $k_{x,mn}$ is the axial mode coefficient in the condition of azimuthal mode number m and radial mode number n; $row(j)$ means that the j-th reflecting wave mode corresponds to the $row(j)$-th "cut-on" mode; N_R is the total number of reflecting wave modes; $\boldsymbol{Q}_{BG}$ is the given fan face vector. The superscript L means the left eigenvector of Eq.(5) at the fan face while the superscript R means the right eigenvector.